Title
Reversed shear Alfvén eigenmode stabilization by localized electron cyclotron heating

Journal
Plasma Physics and Controlled Fusion, 50(3)

ISSN
0741-3335

Authors
Van Zeeland, MA
Heidbrink, WW
Nazikian, R
et al.

Publication Date
2008-03-01

DOI
10.1088/0741-3335/50/3/035009

Plasma Phys. Control. Fusion **50** (2008) 035009 (10pp) doi:10.1088/0741-3335/50/3/035009

Reversed shear Alfvén eigenmode stabilization by localized electron cyclotron heating

M A Van Zeeland[1], W W Heidbrink[2], R Nazikian[3], W M Solomon[3], M E Austin[4], H L Berk[5], N N Gorelenkov[3], C T Holcomb[6], A W Hyatt[1], G J Kramer[3], J Lohr[1], M A Makowski[6], G R McKee[7], C C Petty[1], S E Sharapov[8] and T L Rhodes[9]

[1] General Atomics, PO Box 85608 San Diego, CA 92186-5608, USA
[2] University of California-Irvine, Irvine, CA 92697, USA
[3] Princeton Plasma Physics Laboratory, Princeton, NJ 08543-0451, USA
[4] University of Texas-Austin, Austin, TX 78712, USA
[5] Institute for Fusion Studies, University of Texas at Austin, Austin, TX 78712, USA
[6] Lawrence Livermore National Laboratory, Livermore, CA, USA
[7] University of Wisconsin-Madison, Madison, WI 53726, USA
[8] Euratom/UKAEA Fusion Association, Culham, Abingdon, Oxfordshire, OX14 3DB, UK
[9] University of California-Los Angeles, Los Angeles, California, 90095, USA

E-mail: vanzeeland@fusion.gat.com

Received 17 October 2007, in final form 8 January 2008
Published 7 February 2008
Online at stacks.iop.org/PPCF/50/035009

Abstract

Reversed shear Alfvén eigenmode (RSAE) activity in DIII-D is stabilized by electron cyclotron heating (ECH) applied near the minimum of the magnetic safety factor ($q_{\min}$) in neutral beam heated discharges with reversed-magnetic shear. The degree of RSAE stabilization, fast ion density and the volume averaged neutron production (S_n) are highly dependent on ECH deposition location relative to $q_{\min}$. While discharges with ECH stabilization of RSAEs have higher S_n and more peaked fast ion profiles than discharges with significant RSAE activity, neutron production remains strongly reduced (up to 60% relative to TRANSP predictions assuming classical fast ion transport) even when RSAEs are stabilized.

(Some figures in this article are in colour only in the electronic version)

1. Introduction

Future burning plasma experiments will be subject to the excitation of Alfvénic instabilities by several fast ion sources including both fusion born alpha particles as well as 1 MeV neutral beam ions [1,2]. The ability of these instabilities to cause fast ion transport is well documented [3] as are both the deleterious effects and potentially positive aspects of this transport [4]. While much

attention is focused on gaining a predictive capability for these instabilities in future devices through modeling and extrapolation of current experimental results, far less attention has been paid to intervention and control techniques. A 'knob' capable of turning off a particular type of Alfvénic oscillation is extremely advantageous. Such a control technique could be used to prevent excessive fast ion loss and vessel damage resulting from Alfvén eigenmodes (AEs), while still taking advantage of possible desirable effects. Additionally, in terms of near-term scientific goals, this affords the opportunity to probe the properties of specific instabilities.

Tokamak discharges with reversed-magnetic shear offer several advantages over normal shear such as the formation of internal transport barriers with strong pressure peaking [5, 6], however they are also potentially more susceptible to Alfvénic instabilities due to the fact that eigenmodes localized near the shear reversal point can exist with reduced damping. One particular type of Alfvén eigenmode called the reversed shear Alfvén eigenmode (RSAE) or Alfvén cascade localized near the minimum of the magnetic safety factor ($q_{\min}$) has been the subject of extensive recent research [7–9]. The RSAE is basically a cylindrical mode with toroidal mode number (n) and one dominant poloidal harmonic (m). The RSAE appears when $q_{\min} \approx m/n$, and for a decreasing $q_{\min}$, a second poloidal harmonic $m-1$ increases in amplitude until $q_{\min} = (m-1/2)/n$, at which point the RSAE becomes a toroidicity induced Alfvén eigenmode (TAE) [9, 10]. Throughout this transition, the mode's frequency increases to the local TAE frequency, $f_{\mathrm{TAE}} = V_{\mathrm{A}}/4\pi q_{\mathrm{TAE}} R$, where $q_{\mathrm{TAE}} = (m-1/2)/n$, V_{A} is the Alfvén speed and R is the major radius. Finite plasma pressure effects can alter the mode's existence as well as the minimum frequency of the RSAE [11–14].

This paper documents an experiment carried out on the DIII-D tokamak using electron cyclotron heating (ECH) in a reversed-magnetic shear discharge with neutral beam injection (NBI) to directly alter both the electron temperature (T_{e}) and electron temperature gradient (∇T_{e}) near $q_{\min}$. As stated above, near rational values of $q_{\min}$, both the Alfvén continuum and RSAE are strongly modified by finite pressure effects. Toroidal geometry prevents shear Alfvén waves from being strictly incompressible; instead, they produce a geodesic pressure perturbation which has been the subject of several theoretical studies [12–16]. The use of ECH in these experiments is an attempt to experimentally investigate the dependence of the RSAE on the electron component of the bulk plasma pressure. From the standpoint of targeting and perturbing a particular type of fluctuation with a known location, ECH is an ideal tool since it can provide highly localized targeted power deposition [17].

The key result presented here is that for ECH deposition near the location of $q_{\min}$, the RSAEs are essentially stabilized. However, the TAEs resulting from the RSAE to TAE transitions remain and other global TAEs are also unstable. In terms of fusion performance, discharges with decreased RSAE activity behave closer to TRANSP [18] neutron predictions which assume classical beam ion diffusion; however, a significant deficit in neutron production remains. Discharges with reduced AE activity also have up to 50% higher fast ion density near the magnetic axis as measured by Doppler shifted D-alpha emission.

2. Experimental observation of RSAE stabilization

The target discharge used in this experiment is very similar to the well documented #122117 in which several types of Alfvén eigenmodes (TAEs, RSAEs and ellipticity induced Alfvén eigenmodes (EAEs) [19]) are present and have been studied in detail [20–22]. The major difference is that during the current rise phase of this discharge when 4.6 MW, of sub-Alfvénic (78 keV) neutral deuterium beams are injected and the central magnetic shear is reversed, $\approx$1.9 MW of 110 GHz ECH power is also deposited with radial launch to heat the electrons and drive no net current. A typical equilibrium magnetic flux surface reconstruction overlayed

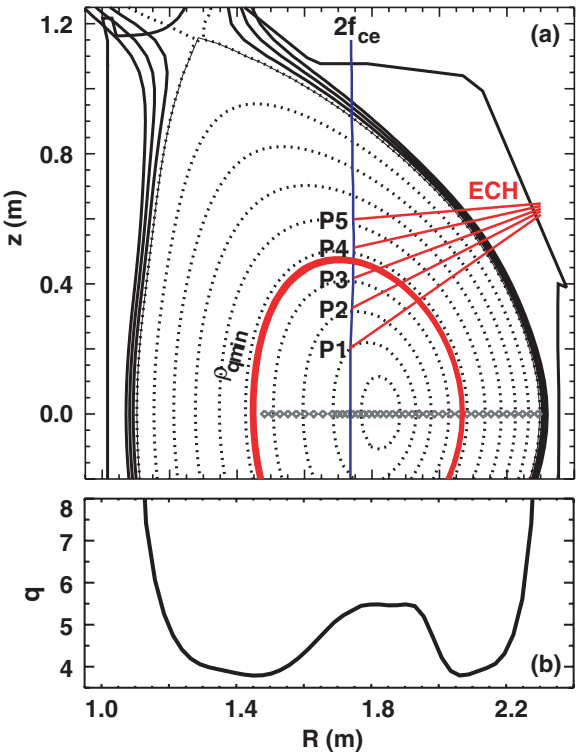

Figure 1. (*a*) Representative equilibrium reconstruction showing $2f_{ce}$ location (blue), ECH deposition locations $P1$–$P5$ ($\rho \approx 0.2$–0.6) (red), ECE radiometer channel locations (gray diamonds) and approximate location of q_{min} surface ($\rho_{q_{min}} \approx 0.4$–$0.5$). $B_T = 2.0\,T$ (*b*) q-profile at $z = 0$.

with the ECH trajectories used in this experiment is shown in figure 1(*a*). The safety factor profile [$q(R)$ at $z = 0$] determined from motional Stark effect (MSE) polarimetry is shown in figure 1(*b*). In a sequence of discharges the ECH deposition location was stepped from $P1$ to $P5$ ($\rho \approx 0.2$–0.6, where ρ is the normalized square root of toroidal flux) as well as deposited at multiple locations during the same discharge. The actual ECH deposition location is at slightly larger minor radius than shown due to refraction effects. The approximate location of $\rho_{q_{min}}$ (where the RSAE are peaked) is also shown along with the location of the radial electron cyclotron emission (ECE) radiometer array channels. The rationale behind the varied ECH deposition locations was to scan for a region of maximum effect—anticipated to be near q_{min}. ECH deposition on either side of q_{min} produces the maximum local change in ∇T_e at q_{min} while deposition with equal power densities on adjacent sides of q_{min} is used to hold ∇T_e approximately constant while raising the local value of T_e.

The suppression of RSAE activity when ECH is deposited near $\rho_{q_{min}}$ is shown in figures 2 and 3, where crosspower spectra of vertical and radial CO_2 interferometer chords are shown. Taking the crosspower of these two chords helps to eliminate localization effects and yields a global picture of the overall Alfvénic activity by observation of the AE induced density perturbation. ECH and NBI are both turned on at $t = 300\,ms$. Figures 2(*a*)–(*c*) are for different ECH deposition locations, i.e. $P1$ ($\rho \approx 0.2$), $P3$ ($\rho \approx 0.45$) and $P2$ & $P4$ from figure 1, respectively. $P2$ & $P4$ indicates simultaneous deposition at the two locations with 0.95 MW at $P2$ ($\rho \approx 0.3$) and 0.95 MW of ECH at $P4$ ($\rho \approx 0.55$). Each of these spectra show

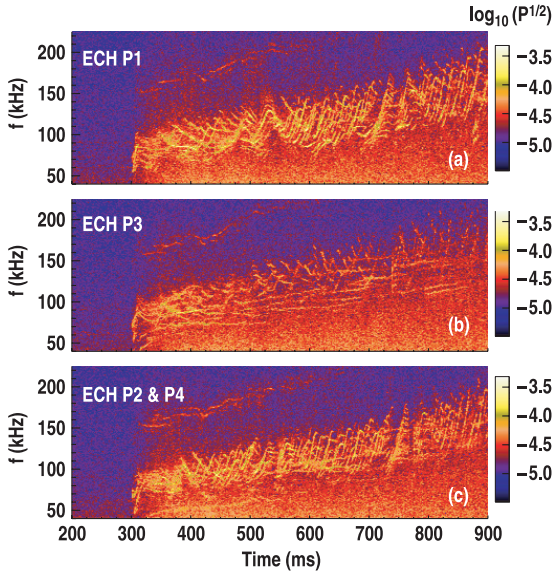

Figure 2. Windowed crosspower spectra of vertical and radial CO_2 interferometer data for 1.9 MW ECH deposition at (*a*) *P*1 #128564, (*b*) *P*3 #128560, (*c*) *P*2 & *P*4 #128562.

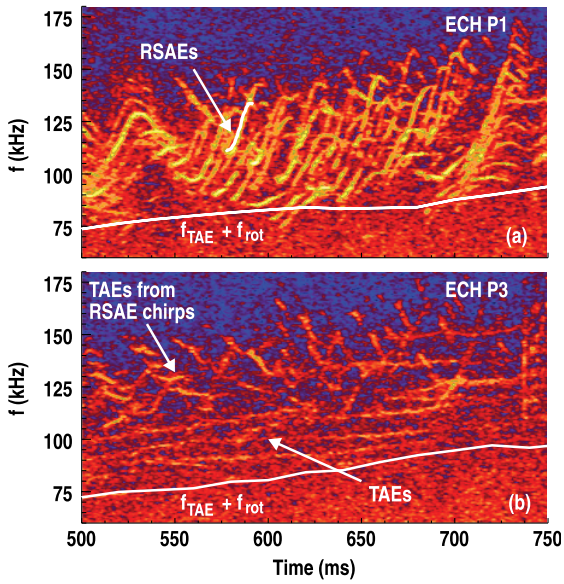

Figure 3. Enlarged region of figure 2. Windowed crosspower spectra of vertical and radial CO_2 interferometer data for 1.9 MW ECH deposition at (*a*) *P*1 #128564, (*b*) *P*3 #128560. Overlayed white curves are a typical RSAE and the local TAE frequeny plus toroidal rotation frequency at $q_{\min}$.

a variety of Alfvén eigenmodes typical for this type of discharge, the majority of which have been discussed in detail previously [20, 22]. The primary difference between these discharges is the dramatic lack of RSAE activity for ECH deposition at *P*3, i.e. just inside of $q_{\min}$. In figure 2(*b*), only the very end of RSAE chirps are visible and are thought to be the point at which the RSAEs have almost completely transitioned to TAEs; a feature which is pointed out

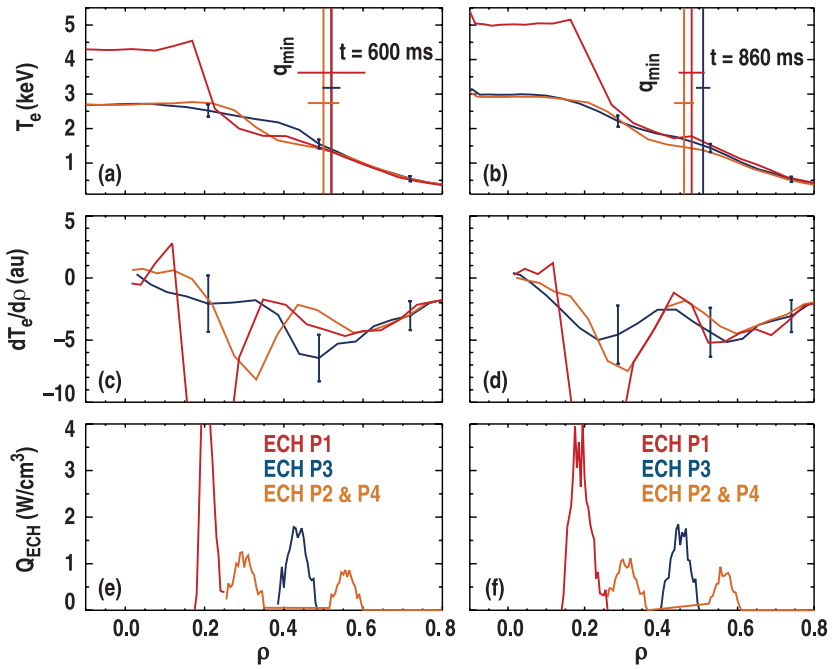

Figure 4. Measured T_e, ∇T_e and Q_{ECH} profiles for ECH deposition locations: $P1$ (red), $P3$ (blue), $P2$ & $P4$ (orange) at two different times (*a*), (*c*), (*e*) $t = 600$ ms, $T_i(0) = 1.07$, 1.45 and 1.23 keV, $n_e(0) = 2.5$, 2.4, 2.5×10^{13} cm^{-3} ($P1$, $P3$, $P2$ & $P4$), (*b*), (*d*), (*f*) $t = 860$ ms, $T_i(0) = 1.41$, 1.63 and 1.56 keV, $n_e(0) = 2.9$, 2.7, 2.8×10^{13} cm^{-3} ($P1$, $P3$, $P2$ & $P4$).

in figure 3. In all panels, the modes beginning at approximately 150 kHz are EAEs [19, 23], which appear to remain unchanged.

To aid the reader with identification of the relevant modes as well as the primary effect of the ECH on the AE behavior, enlarged regions of figures 2(*a*) and (*b*) are shown in figures 3(*a*) and (*b*), where the combined local TAE frequency and toroidal rotation frequency near q_{min} ($f_{TAE} + f_{rot}$) is overlayed as well as a typical RSAE highlighted. The overplotted $f_{TAE} + f_{rot}$ represents the approximate expected frequency of an $n = 1$ TAE near q_{min} and serves to accentuate the difference in the spectral behavior of RSAEs and TAEs. The majority of the TAEs shown are $n > 1$ and will be Doppler shifted to larger frequencies given approximately by $f_{TAE} + nf_{rot}$. As pointed out in the figure, the modes chirping up in frequency on the timescale of 10–20 ms are RSAEs and the relatively constant frequency modes are global TAEs or the TAEs resulting from the RSAE to TAE transition. Other low level TAEs have emerged in the discharge shown in figure 3(*b*) and are seen as a series of modes with slowly varying frequencies in the range just above the overplotted TAE frequency.

The primary effect of the ECH is shown in figures 4(*a*)–(*d*) where radial profiles of the electron temperature and electron temperature gradient from ECE data are given for two different timeslices during the RSAE suppression window from figure 2. Several representative error bars on $T_e(\rho)$ and $dT_e/d\rho$ are shown for discharge 128560 and are similar for all others. The dominant error in the T_e determination is due to an uncertainty associated with the calibration of the ECE radiometer to the ECE Michelson interferometer system. The errors in the gradient are determined using a Monte Carlo approach and represent a conservative estimate given that each radiometer channel is calibrated relative to one another. Also shown in figure 4 is the location of q_{min} from EFIT equilibrium reconstructions that

include MSE measurements as well as thermal pressure data as constraints. The $q_{\min}$ locations have some uncertainty, the approximate magnitudes of which are represented by the overlayed horizontal bars. For discharges with RSAE activity, the ECE channels corresponding to their peak signal is consistent with the location of $q_{\min}$ from MSE [20]. The ECH deposition profiles, as calculated by the TORAY-GA ray tracing code, for the two different times are shown in figures 4(*e*) and (*f*). The error with the calculated deposition profile peak location is extremely small, however, the location relative to $q_{\min}$ is the important factor and is determined by the error bars on $\rho_{q_{\min}}$ shown in figures 4(*a*) and (*b*). For ECH deposition at small minor radius ($P1$), a much larger central T_e results due to the fact that the deposition volume is very small and the total deposited power is held fixed. For the case of deposition at $P3$, where reduced RSAE activity was observed, the electron temperature as well as $|\nabla T_e|$ in the region of $q_{\min}$ is slightly higher than for deposition at $P1$ and $P2$ & $P4$ throughout much of the current rise phase, but is very close by $t = 860$ ms.

3. Discussion of RSAE stabilization

Several sources for the RSAE stabilization shown in figures 2(*b*) and 3(*b*) are considered, however, the exact stabilization mechanism is not currently known. Recent work on NSTX [24] and MAST [25] hypothesize that the lack of RSAE activity in spherical tokamak (ST) plasmas is due to β stabilization in which the geodesic acoustic frequency (and Alfvén continuum near $q_{\min}$) given by

$$f_g = \frac{1}{2\pi}\left[\frac{2}{M_i R^2}\left(T_e + \frac{7}{4}T_i\right)\right]^{1/2} \tag{1}$$

is very close to, or higher than f_{TAE} 'leaving no frequency band for the RSAE to exist' [24]. In equation (1), M_i is the ion mass, T_i ion temperature, T_e electron temperature and R the major radius.

Both the RSAE's minimum frequency (f_m) and existence, however, have been shown to not only depend on the local GAM frequency, but the plasma pressure gradient [11, 13, 14] and fast ion density gradient [9] as well. Recent work by Breizman [26] collects the work of several sources [9–11, 13, 14] and summarizes all of these different effects in the limit of high n and m leading to an approximation for f_m given by

$$f_m^2 = f_g^2 + f_{\nabla T}^2 + f_{\nabla FI}^2, \tag{2}$$

where

$$f_{\nabla T}^2 = \frac{-1}{2\pi^2 M_i R^2}\rho\frac{d}{d\rho}(T_e + T_i), \tag{3}$$

$$f_{\nabla FI}^2 = \frac{-f_m}{4\pi^2 m}\left|\frac{eB}{M_i c}\right|\frac{\rho}{n_{plasma}}\frac{d}{d\rho}n_{fast}. \tag{4}$$

In equations (3) and (4) above, m is the poloidal mode number, n_{plasma} is background plasma density and n_{fast} is the fast ion density, respectively. Also, all quantities are evaluated at $q_{\min}$ and the radial derivatives have been modified from [26, 27] to be taken with respect to normalized square root of toroidal flux (ρ).

The temporal evolution of f_{TAE}, f_g and $(f_g^2 + f_{\nabla T}^2)^{1/2}$, as well as the toroidal rotation frequency (f_{rot}) near $q_{\min}$ for the discharges of figure 2 are shown in figure 5. Unlike the ST results, f_g is much smaller than f_{TAE} for all discharges. Inclusion of the thermal plasma gradient term ($f_{\nabla T}$) raises the minimum RSAE frequency significantly; the largest change is apparent in the discharge with RSAE suppression, i.e. ECH at $P3$, where $(f_g^2 + f_{\nabla T}^2)^{1/2}$, reaches f_{TAE}

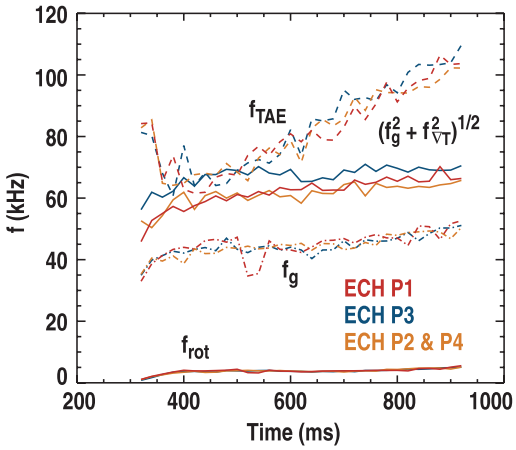

Figure 5. Various frequencies evaluated at $q_{\min}$. Dashed = $f_{\rm TAE}$, solid = $(f_{\rm g}^2 + f_{\nabla {\rm T}}^2)^{1/2}$, dash–dot = f_g, dash–dot–dot = $f_{\rm rot}$. ECH deposition locations: $P1$ (red), $P3$ (blue), $P2$ & $P4$ (orange).

at early times. However, even for deposition at $P3$, there is a large separation of $f_{\rm m}$ and $f_{\rm TAE}$ at later times ($t > 550$ ms) when the modes are still absent from the spectra. The contribution due to fast ions ($f_{\nabla {\rm FI}}$) is not shown in figure 5 due to the extremely large uncertainties associated with $n_{\rm fast}$. Conservative estimates for $n_{\rm fast}$, however, show that this term is comparable to or larger than $f_{\nabla {\rm T}}$, making it possible that a similar stabilizing effect to that discussed in the context of ST plasmas is occurring here.

An alternative mechanism for stabilization that needs to be considered is the modification of the effective electron collisionality that can change Alfvén wave damping from electrons. A larger effective collisionality may be present due to the stochastic electron scattering inherent in the ECH interaction. The interaction with the rf wavefield may also create an increased population of trapped electrons. Both of these effects are likely to enhance what would otherwise be denoted as electron collisional damping. A quantitative analysis of, however, needs to be developed. Changes in both the beam ion distribution from the ECH altered slowing down time and enhanced transport as well as ECH modification of the effective collision frequencies will certainly alter the stability properties and saturation of these modes and will be treated in future work.

4. Impact of RSAE stabilization

There is evidence for improved beam ion confinement in the discharges with ECH deposition near $q_{\min}$ and stabilized RSAEs. As a measure of the level of Alfvénic activity, figure 6(a) shows the temporal evolution of the integrated power in the TAE/RSAE range (50–230 kHz) of the CO_2 interferometer data presented in figure 2. These data represent the level of AE induced density fluctuations. Other methods of quantifying the level of AE activity such as Mirnov coils and ECE radiometer measurements have also been used and all essentially produce similar results. The largest error associated with an approach such as this is that each method has an instrument function that preferentially sees some modes rather than others. To deal with this, the crosspower of two different interferometer chords was used which reduces the susceptibility to, for example, line-averaging effects.

Figure 6(b) shows the relative impact on volume averaged neutron production compared to TRANSP simulations which assume classical beam ion orbits. Since the primary source

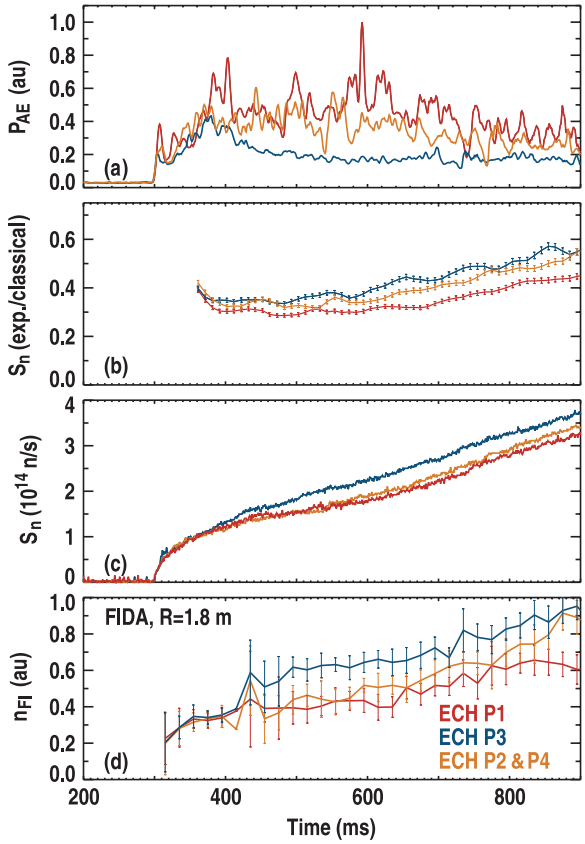

Figure 6. (*a*) Integrated band-pass filtered density fluctuation level (from figure 2) in TAE/RSAE frequency range (*b*) neutron emission relative to TRANSP predictions. (*c*) Fast ion density measured by FIDA diagnostic near magnetic axis ($R = 1.8$ m).

of neutrons in these discharges is from beam-plasma or beam-beam and the density profile is centrally peaked, a number less than one indicates a non-classical redistribution or loss of the fast ions. Discharge #128560 with ECH deposition near $q_{\min}$ and stabilized RSAE activity has higher S_n (scaled to TRANSP predictions as well as unscaled, see figure 6(*c*)) than discharges with significant RSAE activity. This increased neutron emission when scaled to TRANSP predictions can only be due to a reduced fast ion transport. An interesting point however, is that up to 60% of the S_n reduction remains, indicating that the bulk of the neutron deficit is not due to RSAE activity in these discharges. The error bars shown in figure 6(*b*) were derived through a series of TRANSP runs. In order to do this, an ensemble of input profiles for each timestep were arrived at by randomly perturbing all measurements within their errorbars and recalculating new spline fits.

In figure 6(*c*) the unscaled volume averaged neutron rate is given which clearly shows a significantly larger neutron emission in the discharge with ECH injection at $P3$. Additionally, the neutron emission of the three discharges shown is nearly identical until approximately $t = 380$ ms at which time the level of Alfvénic activity begins to deviate between discharges. The random error on the measured neutron emission is small and is similar in magnitude to the high frequency fluctuations apparent in the time traces shown in figure 6(*c*). This small random error is the primary source of error in determining the fraction change in

S_n from discharge to discharge As a result, the relative comparison of the discharges in figure 6(*c*) is extremely reliable. The uncertainty in absolute calibration, however, which changes on much longer timescales and does not affect shot to shot variation, is larger and approximately 15%.

Further evidence of improved fast ion confinement, and perhaps the most straightforward, is given in figure 6(*d*), which shows fast ion D-alpha (FIDA) measurements [28] near the magnetic axis of the density of full-energy beam ions (n_{FI}). These data are found by integrating localized measurements of Doppler shifted D-alpha light over wavelengths that correspond to perpendicular ion energies of $E_\lambda = 30$–60 keV. Similar to the neutron measurements, n_{FI} is smallest for ECH deposition at $P1$. In terms of fast ion density, this is in contrast to what one would expect based purely on neutral beam ions slowing down classically due to electron drag. With the higher central T_e for ECH deposition near the axis, one would expect larger fast ion density on-axis. This is clearly not the case and the increased fast ion density on-axis for ECH deposition near q_{min} is attributed to reduced fast ion radial transport in the discharges with little or no RSAE. Interestingly, before $t \approx 400$ ms, when the overall level of Alfvénic activity is similar in all three discharges, so is the measured fast ion density. Additionally, not shown in figure 6, FIDA measurements show that discharges with suppressed AE activity have more centrally peaked spatial profiles of n_{FI} as expected if the fast ion transport is reduced. A much more detailed analysis of the fast profile effects due to AEs in DIII-D which includes spatial profiles of these discharges as well as the impact on local momentum confinement is presented in reference [29].

As shown in figure 2(*b*), some coherent mode activity still exists, namely the TAEs from the RSAE to TAE transition as well as other TAEs remain in discharge #128560. It is possible these remaining modes are responsible for the reduced fusion performance occurring in the absence of RSAEs. This finding is consistent with recent measurements on JT-60U where it was found that increased fast ion transport occurs near the final phase of RSAE to TAE transition [30]. Also remaining in these discharges is a significant level of broadband low-k fluctuations, as can be seen in figure 2, that may contribute to enhanced fast ion transport.

5. Conclusions

In summary, initial results from an experiment using ≈1.9 MW of localized ECH to modify RSAE behavior in the DIII-D tokamak has been presented. It has been observed that ECH deposition near q_{min} in a reversed shear discharge stabilizes the RSAEs, while deposition near the magnetic axis or simultaneously on adjacent sides of q_{min} does not stabilize the modes. Analytic estimates of the local RSAE minimum frequency (f_m) based on equilibrium profiles indicate that f_m is below f_{TAE}, particularly at later times when q_{min} has evolved and the stabilization persists. Discharges with stabilized RSAEs have higher volume averaged neutron production and larger relative central fast ion densities than discharges with significant RSAE activity; however, up to 60% S_n reduction remains, indicating that the bulk of the neutron deficit is not due to RSAEs alone.

These recent results prove in principle that RSAEs and other AEs as well as their resultant fast ion transport can be severely affected by localized ECH. It should be pointed out that the use of ECH for the stabilization of RSAEs in DIII-D is not yet a routine control tool. While easily repeated in subsequent discharges with similar plasma conditions, the sensitivity of this mechanism to basic plasma parameters, NBI, and ECH setup has not been evaluated and will be the subject of future work. At this time, the exact stabilization mechanism is not known and, while intriguing, further understanding is required to project the utility of

this method from a limited dataset to its routine use in other plasma conditions and operating scenarios.

Acknowledgments

This work was supported in part by the US Department of Energy under DE-FC02-04ER54698, SC-G903402, DE-AC02-76CH03073, DE-FG03-97ER54415, W-7405-ENG-48, DE-FG02-89ER53296 and DE-FG03-01ER54615.

References

[1] Fu G Y and Van Dam J W 1989 *Phys. Fluids* B **1** 1949
[2] Gorelenkov N N *et al* 2003 *Nucl. Fusion* **43** 594
[3] Wong K L 1999 *Plasma Phys. Control. Fusion* **41** R1
[4] Wong K L *et al* 2004 *Phys. Rev. Lett.* **93** 085002
[5] Levington F M *et al* 1995 *Phys. Rev. Lett.* **75** 004417
[6] Strait E J *et al* 1995 *Phys. Rev. Lett.* **75** 004421
[7] Kusama Y *et al* 1998 *Nucl. Fusion* **38** 1215
[8] Sharapov S E *et al* 2001 *Phys. Lett.* A **289** 127
[9] Berk H L, Borba D N, Breizman B N, Pinches S D and Sharapov S E 2001 *Phys. Rev. Lett.* **87** 1085002
[10] Breizman B N *et al* 2003 *Phys. Plasmas* **10** 3649
[11] Kramer G J, Gorelenkov N N, Nazikian R M and Cheng C Z 2004 *Plasma Phys. Control. Fusion* **46** L23
[12] Breizman B N *et al* 2006 *Phys. Plasmas* **12** 112506
[13] Fu G Y and Berk H L 2006 *Phys. Plasmas* **13** 052502
[14] Gorelenkov N N, Kramer G J and Nazikian R N 2006 *Plasma Phys. Control. Fusion* **48** 1255
[15] Chu M S, Greene J M, Lao L L, Turnbull A D and Chance M S 1992 *Phys. Fluids* B **4** 3713
[16] Turnbull A D *et al* 1993 *Phys. Fluids* B **5** 2548
[17] Lohr J 2002 *Proc. 19th IEEE/IPSS Symp. on Fusion Engineering (SOFE) (Atlantic City, NJ, USA)* p 126
[18] Budny R V 1994 *Nucl. Fusion* **34** 1247
[19] Betti R and Freidberg J P 1991 *Phys. Fluids* B **3** 1865
[20] Van Zeeland M A *et al* 2006 *Phys. Rev. Lett.* **97** 135001
[21] Heidbrink W W 2006 *Proc. 21st IAEA Fusion Energy Conf. (Chengdu, China)* and http://www-pub.iaea.org/MTCD/Meetings/fec2006/ex_6-3.pdf
[22] Van Zeeland M A *et al* 2007 *Phys. Plasmas* **14** 056102
[23] Van Zeeland M A *et al* 2006 *Nucl. Fusion* **46** S880
[24] Fredrickson E *et al* 2007 *Phys. Plasmas* **14** 102510
[25] Pinches S D *et al* 2006 *Proc. 21st Fusion Energy Conf. (Chengdu, China, 16–21 October 2006)* (Vienna: IAEA) Paper EX/7_Ra
[26] Breizman B N 2006 *Theory of Fusion Plasmas: Joint Varenna-Lausanne International Workshop (Varenna, Italy)* CP871
[27] Breizman B N 2007 private conversation
[28] Heidbrink W W *et al* 2007 *Plasma Phys. Control. Fusion* **49** 1457
[29] Heidbrink W W *et al* 2008 *Nucl. Fusion* submitted
[30] Ishikawa M *et al* 2006 *Nucl. Fusion* **46** S898